Exploring Thermospheric Variability and Far-Ultraviolet Airglow Sensitivity: First Results from Ensemble Modeling with the Whole Atmosphere Model

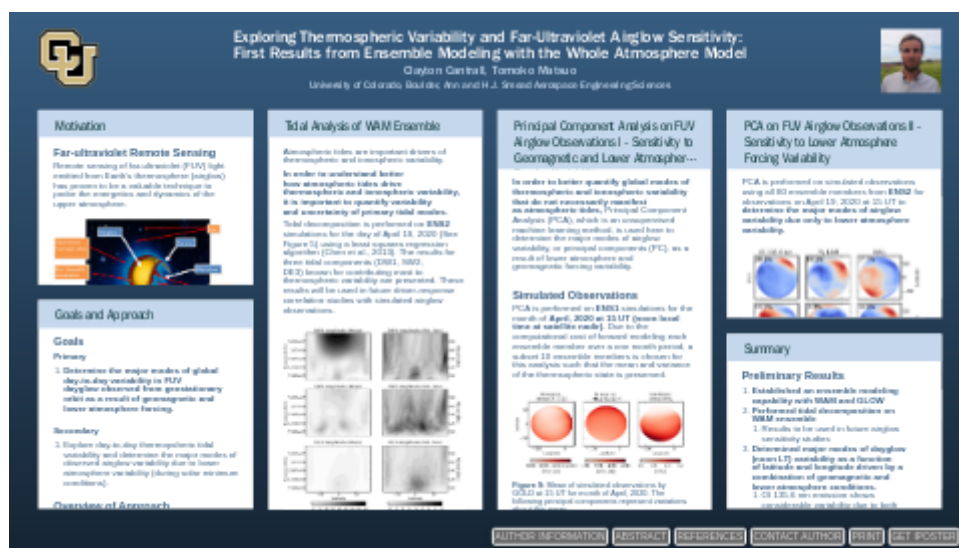Clayton Cantrall[1] and Tomoko Matsuo[1]

[1]University of Colorado Boulder

November 21, 2022

Abstract

Earth's thermosphere is driven by a combination of meteorological, magnetospheric, and solar forcing that exhibits significant variation from day-to-day. The relative importance of these drivers and their combined affects in determining daily thermospheric variability on global and local scales is an important science question particularly under solar minimum conditions. Far-ultraviolet, satellite-based airglow observations are a valuable tool to probe the thermosphere and can provide the spatial coverage and temporal resolution required to improve our understanding of thermospheric day-to-day variability in response to driver variability. This paper presents first results from principal component analysis and ensemble sensitivity analysis to quantify the major modes of dayglow variability in both OI 135.6 nm emissions and N2 Lyman-Birge-Hopfield emissions and the sensitivity of these modes to geomagnetic and lower atmosphere drivers. The ensemble simulations are performed with NOAA's Whole Atmosphere Model that extends from Earth's surface to the exobase and NCAR's Global Airglow Model for a recent period with low-to-moderate levels of geomagnetic activity and low solar activity. The ensemble simulations are compared to thermospheric observations over the same period by the NASA Global-scale Observations of the Limb and Disk (GOLD) mission.

Exploring Thermospheric Variability and Far-Ultraviolet Airglow Sensitivity:
First Results from Ensemble Modeling with the Whole Atmosphere Model

Clayton Cantrall, Tomoko Matsuo

University of Colorado, Boulder, Ann and H.J. Smead Aerospace Engineering Sciences

PRESENTED AT:

MOTIVATION

Far-ultraviolet Remote Sensing

Remote sensing of far-ultraviolet (FUV) light emitted from Earth's thermosphere (airglow) has proven to be a valuable technique to probe the energetics and dynamics of the upper atmosphere.
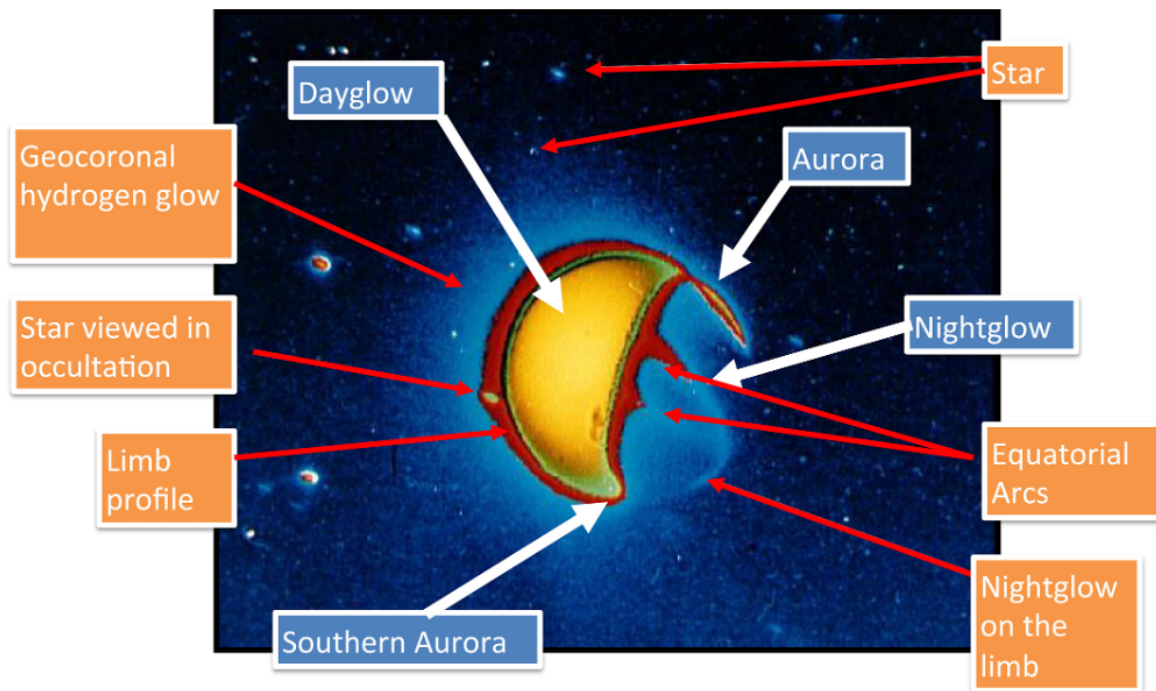

Figure 1: Colorized image of the Earth based on the images from Carruthers and Page [1972] with the most prominent FUV emission processes (Paxton et al., 2017). FUV emissions are sensitive to the major thermospheric constituents (H, O, N_2, N, O_2) and provide insight into important geophysical conditions, including thermospheric composition and temperature, auroral particle precipitation, F region ionospheric O^+, and F region elctrodynamics (Paxton et al., 2017). Figure courtesy of Paxton et al. (2017).

Satellite-based FUV remote sensing of the upper atmosphere has supported important discoveries into the coupling of Earth's lower and upper atmosphere via the upward propagation of solar-thermal tides, gravity waves, and planetary waves.
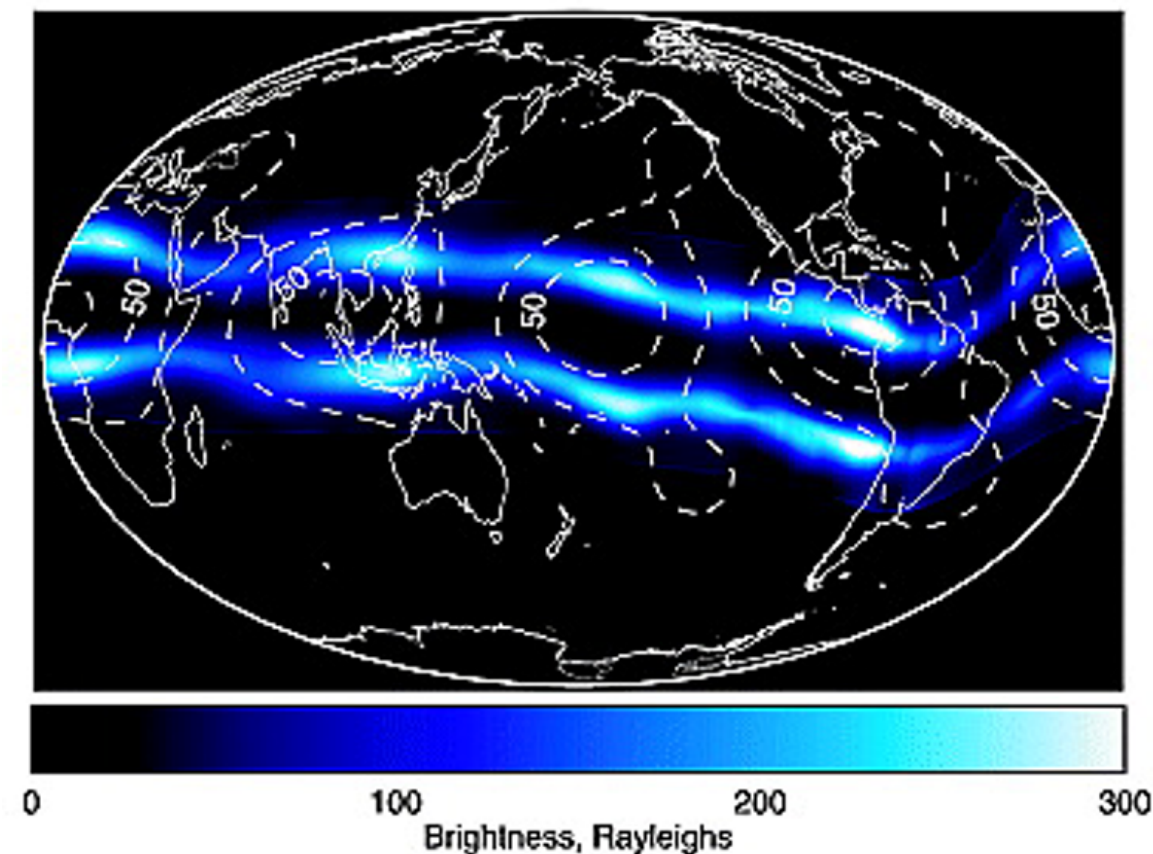
Figure 2: Reconstruction of ultraviolet airglow emitted by the F region equatorial ionization anomaly as measured by the IMAGE satellite. The observed four-peak structure in longitude is likely a result of the upward propogating diurnal eastward wavenumber 3 (DE3) tidal component. Figure courtesy of Immel et al. (2006).

New Perspective in the FUV

There remain many outstanding questions regarding the response of the thermosphere to day-to-day variable solar-geomagnetic and lower atmosphere forcing. Satellite-based airglow observations can provide the spatial coverage and temporal resolution, that has historically been lacking, needed to monitor the evolution of the thermosphere and help resolve these outstanding questions.

The NASA Global-scale Observations of the Limb and Disk (GOLD) mission, launched in 2017, provides an unprecedent, global imaging capability of Earth's FUV airglow from geostationary orbit (Eastes et al., 2017).
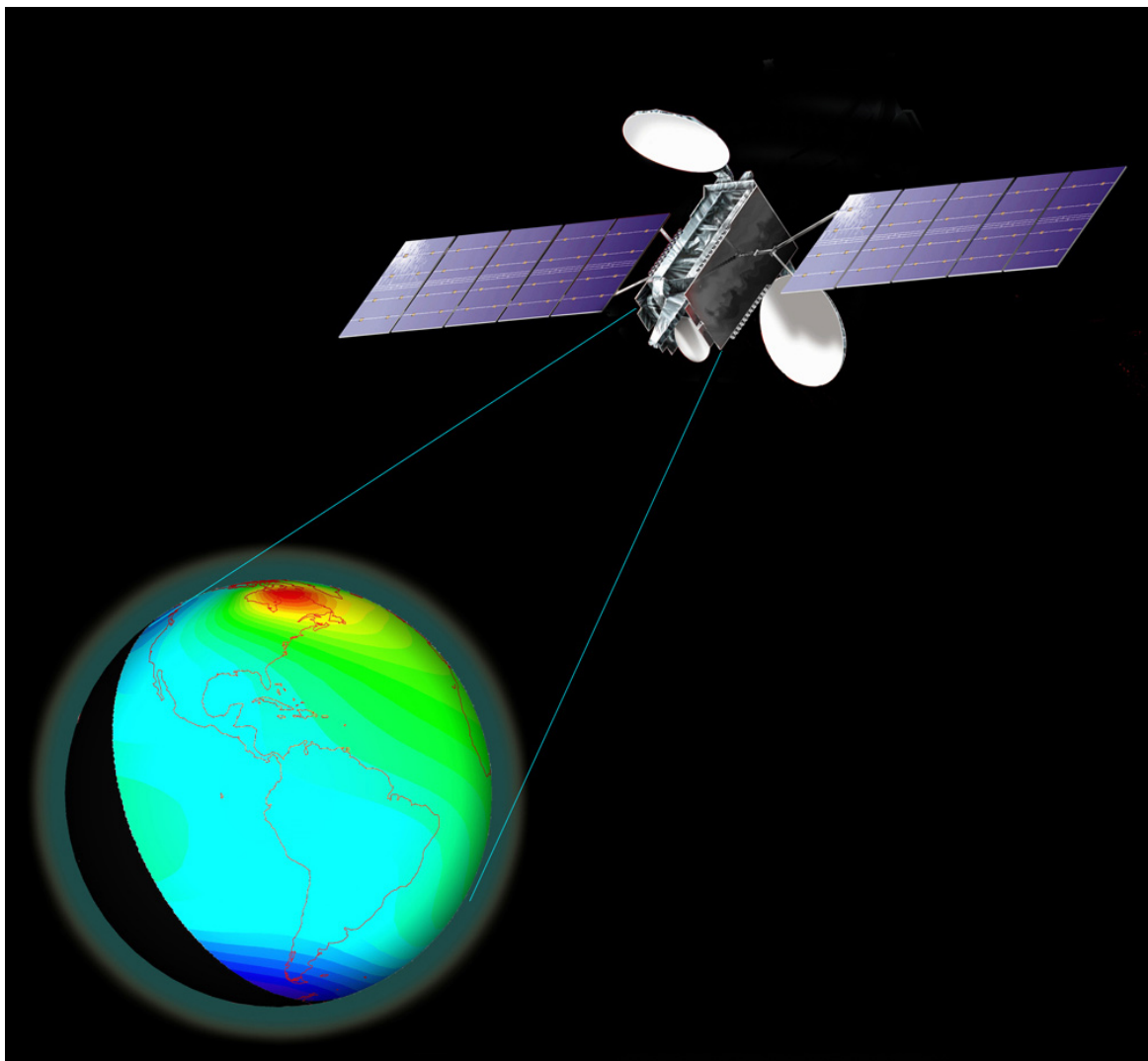
Figure 3: Artist's rendering of Earth's upper atmosphere from GOLD's perspective. Figure courtesy of NASA.

GOALS AND APPROACH

Goals

Primary

1. **Determine the major modes of global day-to-day variability in FUV dayglow observed from geostationary orbit as a result of geomagnetic and lower atmosphere forcing.**

Secondary

1. Explore day-to-day thermopsheric tidal variability and determine the major modes of observed airglow variability due to lower atmosphere variability (during solar minimum conditions).

Overview of Approach

1. Whole atmosphere ensemble simulations

- Tidal Analysis

2. FUV airglow ensemble simulations

- Principal Component Analysis
  - Comparison to GOLD

Whole Atmopshere Model

NOAA's Whole Atmosphere Model (WAM) is an extension of the operational Global Forecast System (GFS) used by the National Center for Environmental Prediction (Akmaev, 2011).

- General circulation model of neutral atmosphere
- Top pressure level: $3x10^{-7}$ Pa (~600 km)
- Weimer model for high latitude electric potential
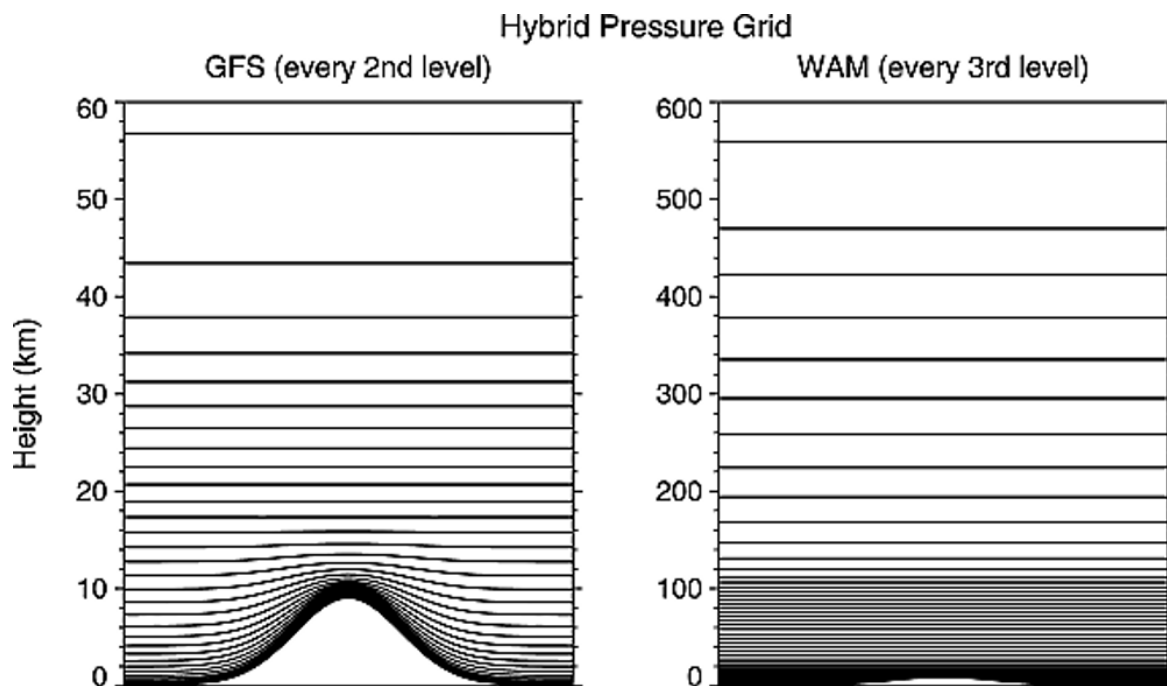- Empirical ionosphere (Chiu, 1975)

Figure 4: Nominal height (kilometers) of midlayer pressure levels over an idealized 9 km bell−shaped mountain for (left) the operational GFS 64−layer grid (every second level shown) and (right) the WAM 150−layer grid (every third level shown). Figure courtesy of Akmaev (2011).

WAM Ensemble Generation

Two 80-member WAM ensembles are generated and denoted as **ENS1** and **ENS2**

1. **ENS1:** geomagnetic drivers <u>and</u> lower atmosphere initial conditions perturbed

2. **ENS2**: <u>only</u> lower atmosphere initial conditions perturbed

Solar EUV drivers are unperturbed and equal to real-time conditions for both ensembles. The simulations ran from March-May, 2020.

Perturbed Geomagnetic Drivers

An ensemble of 80 perturbed geomagnetic conditions is generated by sampling from a Gaussian distribution with a covariance that is computed from the real-time forcing conditions for 6 drivers over a 2 month period, removing spurious correlations (Figure 5).
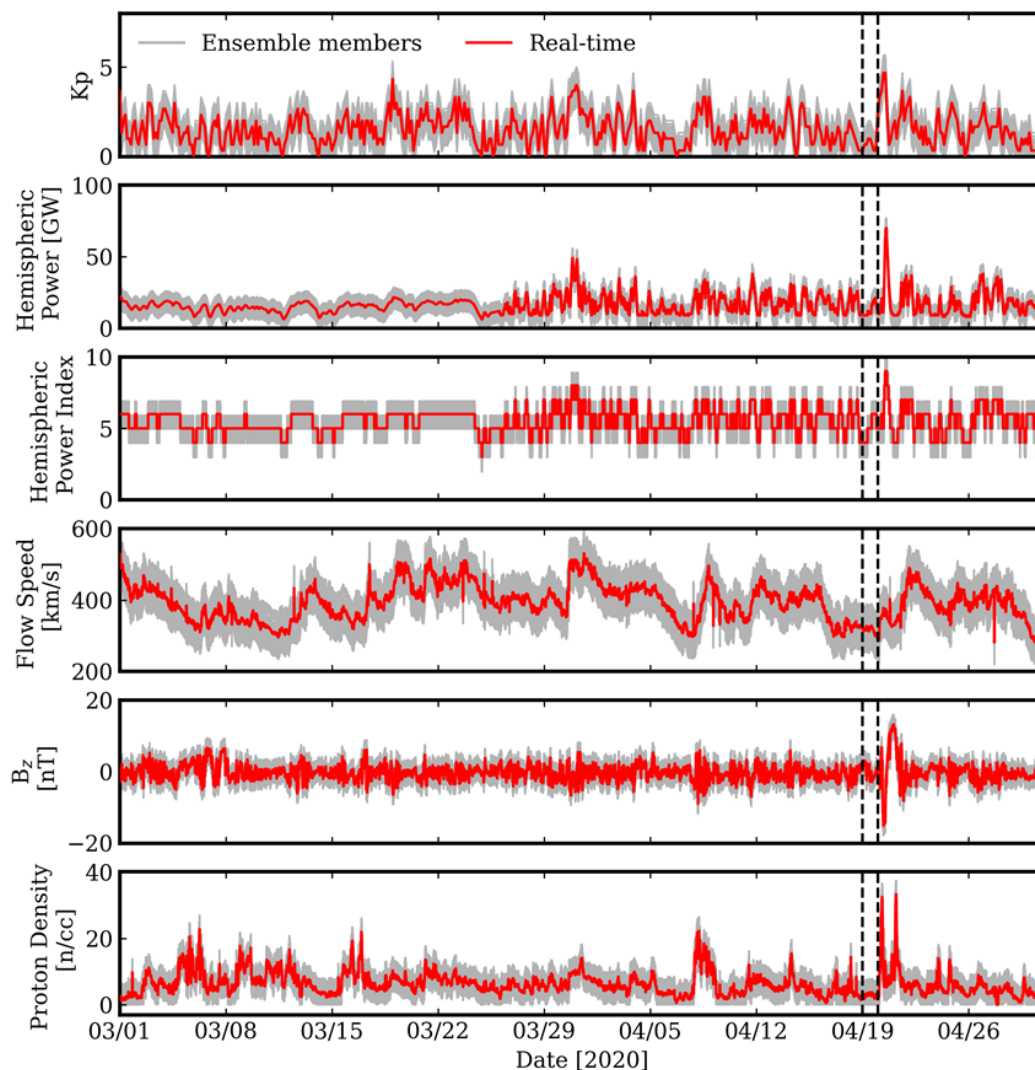
Figure 5: Ensemble of geomagnetic forcing conditions (grey) and real-time conditions (red) over the two month simulation period. The vertical dotted lines define the day that is used in the tidal analysis and airglow sensitivity to lower atmosphere variability study. ENS2 uses the same real-time values for each ensemble member.

Perturbed Lower Atmosphere Initial Conditions

An 80-member ensemble of lower atmosphere initial conditions is generated from the Global Data Assimilation System (GDAS) used by GFS.
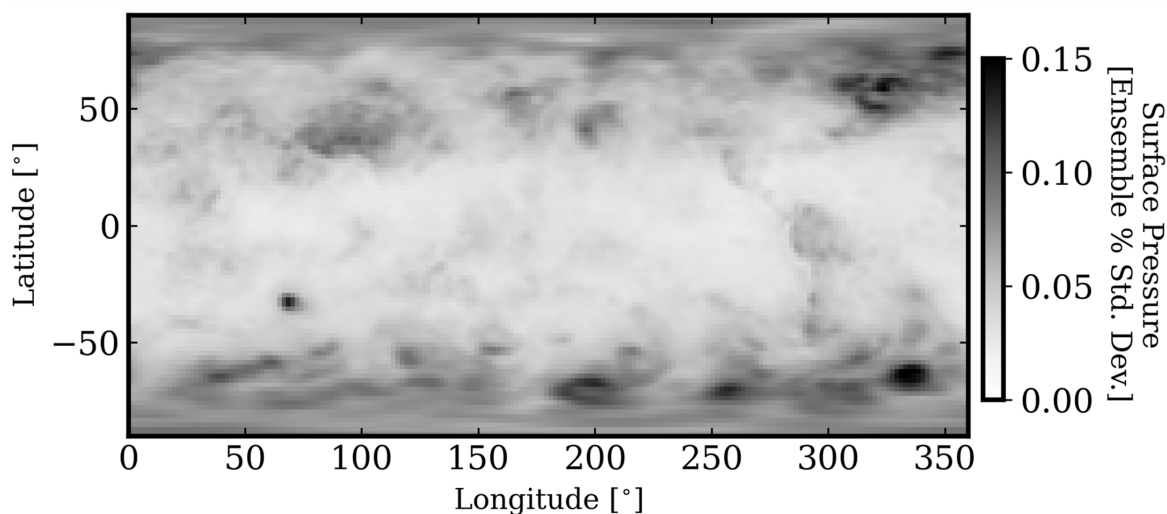
Figure 6: Percent standard deviation of the surface pressure in the initial condition ensemble. Small errors are introduced in the lower atmosphere intial conditions that grow as the simulation progresses due to chaotic divergence and internal atmospheric variability.

Airglow (Forward) Model

The forward model that converts the thermospheric state to synthetic airglow emissions observed by GOLD consists of the NCAR Global Airglow Model (GLOW) and a raditive transfer model (Solomon, 2017).

Primary **dayglow disk** observations

- OI 135.6 nm emission
- N_2 Lyman-Birge-Hopfield (LBH) band emission
- O/N_2 ratio (thermospheric composition)

TIDAL ANALYSIS OF WAM ENSEMBLE

Atmospheric tides are important drivers of thermospheric and ionospheric variability.

In order to understand better how atmospheric tides drive thermospheric and ionospheric variability, it is important to quantify variability and uncertainty of primary tidal modes.

Tidal decomposition is performed on **ENS2** simulations for the day of April 19, 2020 (See Figure 5) using a least squares regression algorithm (Chen et al., 2013). The results for three tidal components (DW1, SW2, DE3) known for contributing most to thermospheric variability are presented. These results will be used in future driver-response correlation studies with simulated airglow observations.
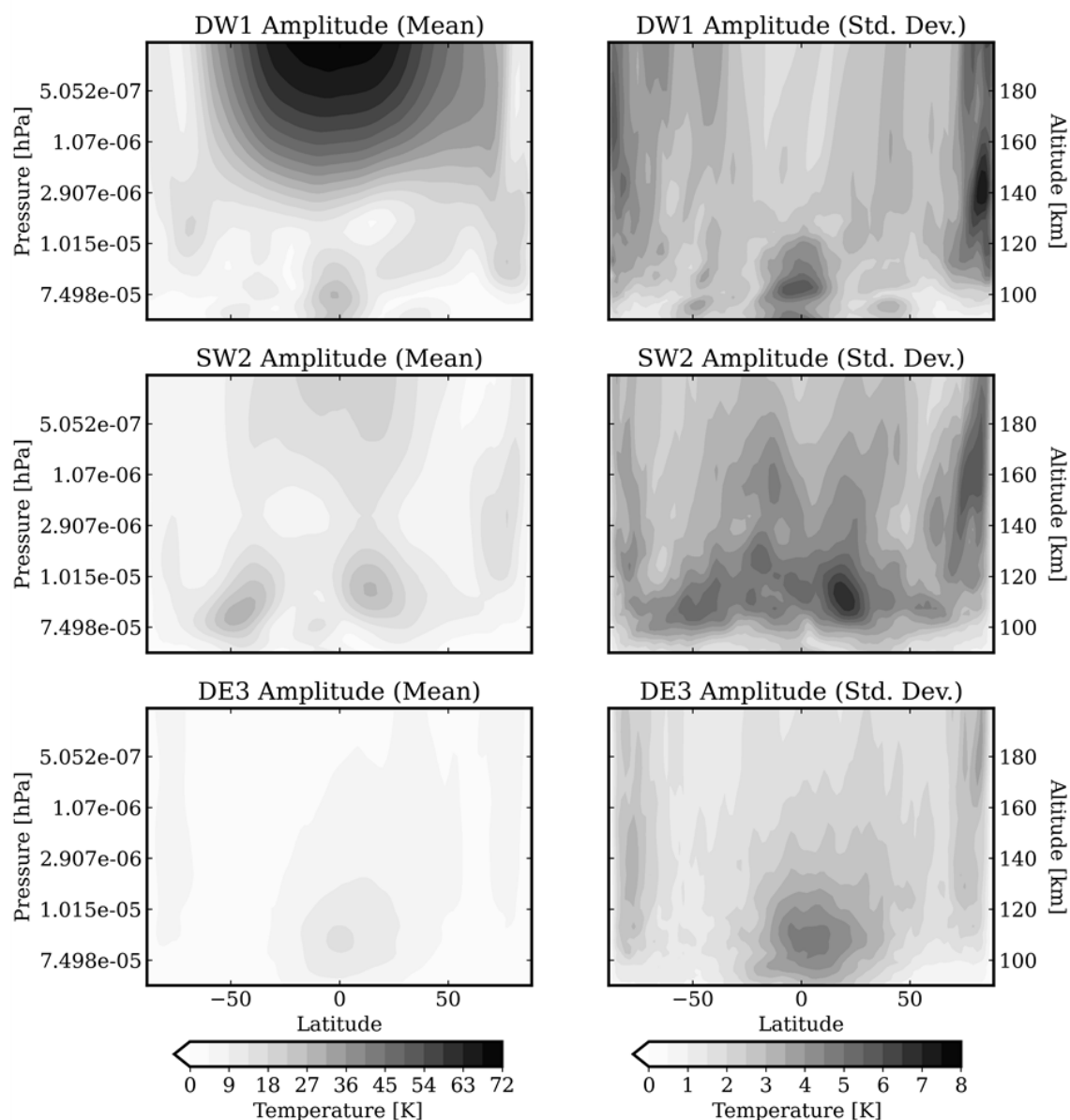

Figure 7: The mean and standard deviation of the DW1 and SW2 migrating tidal amplitudes and the DE3 non-nigrating tidal amplitude on April 19, 2020 as a function of altitude and latitude. The chosen altitude range of 90-200 km approximately spans the region contributing to the top-of-atmosphere airglow observations with the greatest
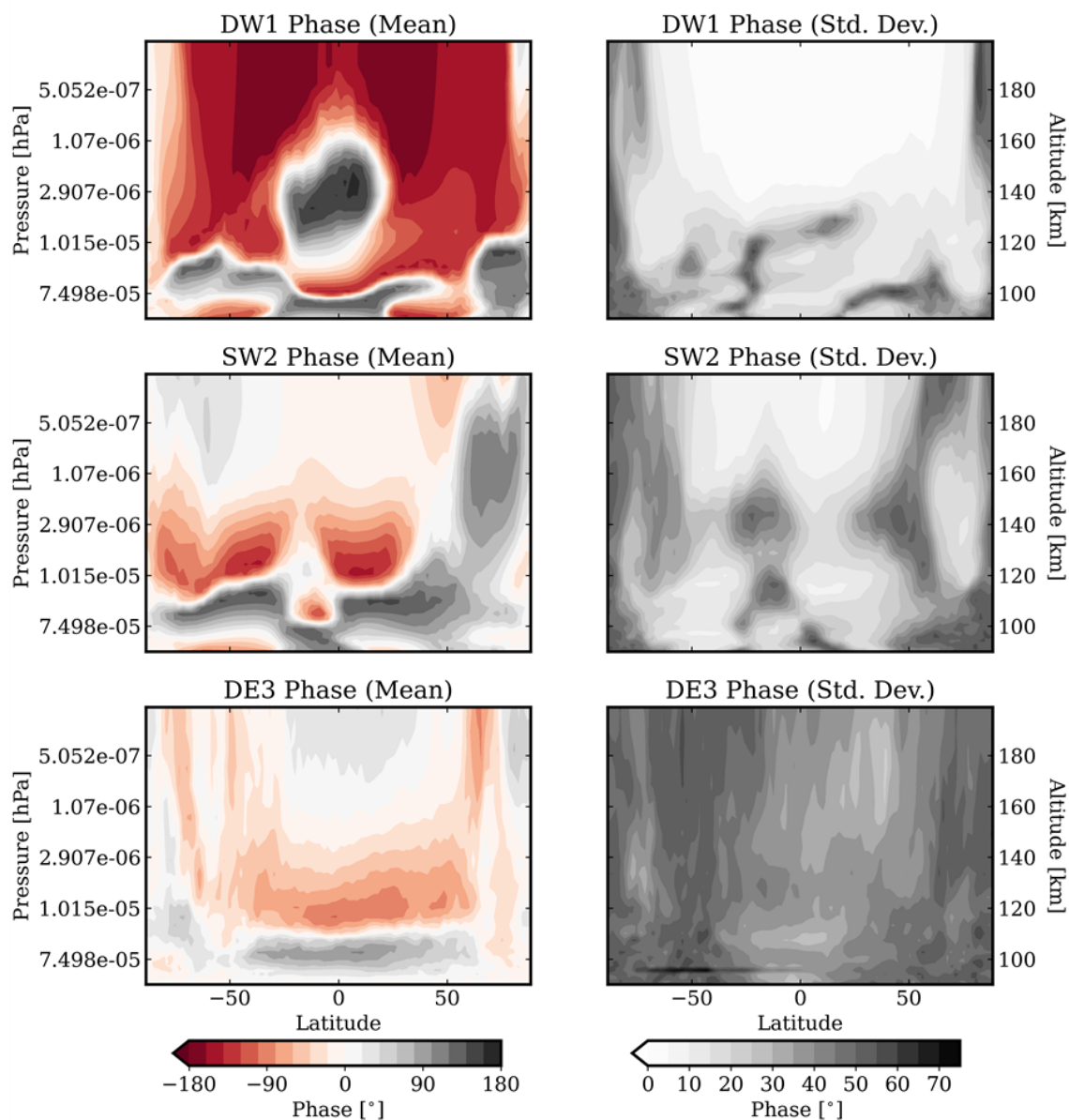
contibution coming from ~150 km altitude.

Figure 8: The mean and standard deviation of the DW1 and SW2 migrating tidal phases and the DE3 non-migrating tidal phase on April 19, 2020 as a function of altitude and latitude. Note that in general the strongest variaiblity in phase occurs where the tidal amplitude is weakest (See Figure 7).

PRINCIPAL COMPONENT ANALYSIS ON FUV AIRGLOW OBSERVATIONS L - SENSITIVITY TO GEOMAGNETIC AND LOWER ATMOSPHERE FORCING VARIABILITY

In order to better quantify global modes of thermospheric and ionospheric variability that do not necessarily manifest as atmospheric tides, Principal Component Analysis (PCA), which is an unsupervised machine learning method, is used here to determine the major modes of airglow variability, or principal components (PC), as a result of lower atmosphere and geomagnetic forcing variability.

Simulated Observations

PCA is performed on **ENS1** simulations for the month of **April, 2020 at 15 UT (noon local time at satellite nadir).** Due to the computational cost of forward modeling each ensemble member over a one month period, a subset 10 ensemble members is chosen for this analysis such that the mean and variance of the thermsopheric state is preserved.
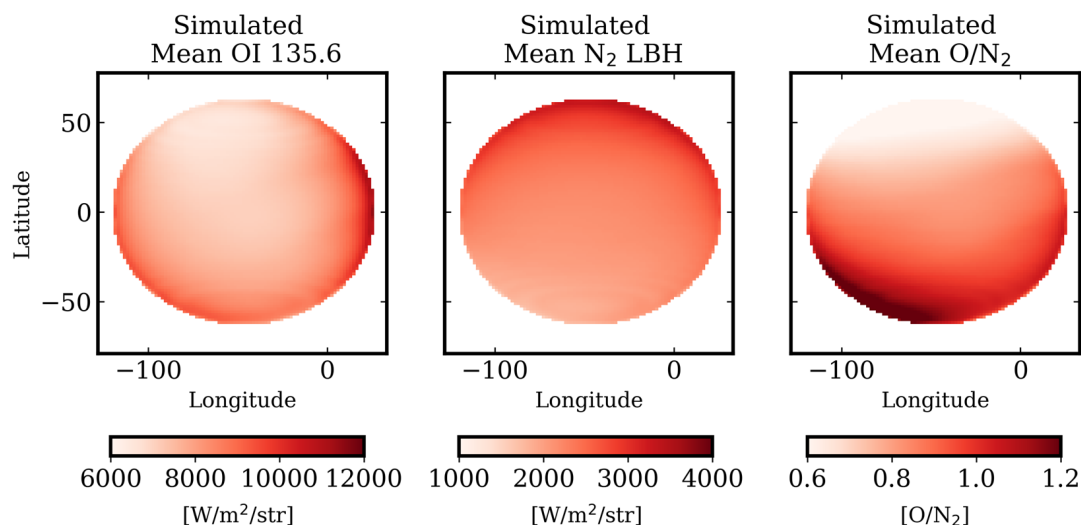

Figure 9: Mean of simulated observations by GOLD at 15 UT for month of April, 2020. The following principal components represent variations about this mean.
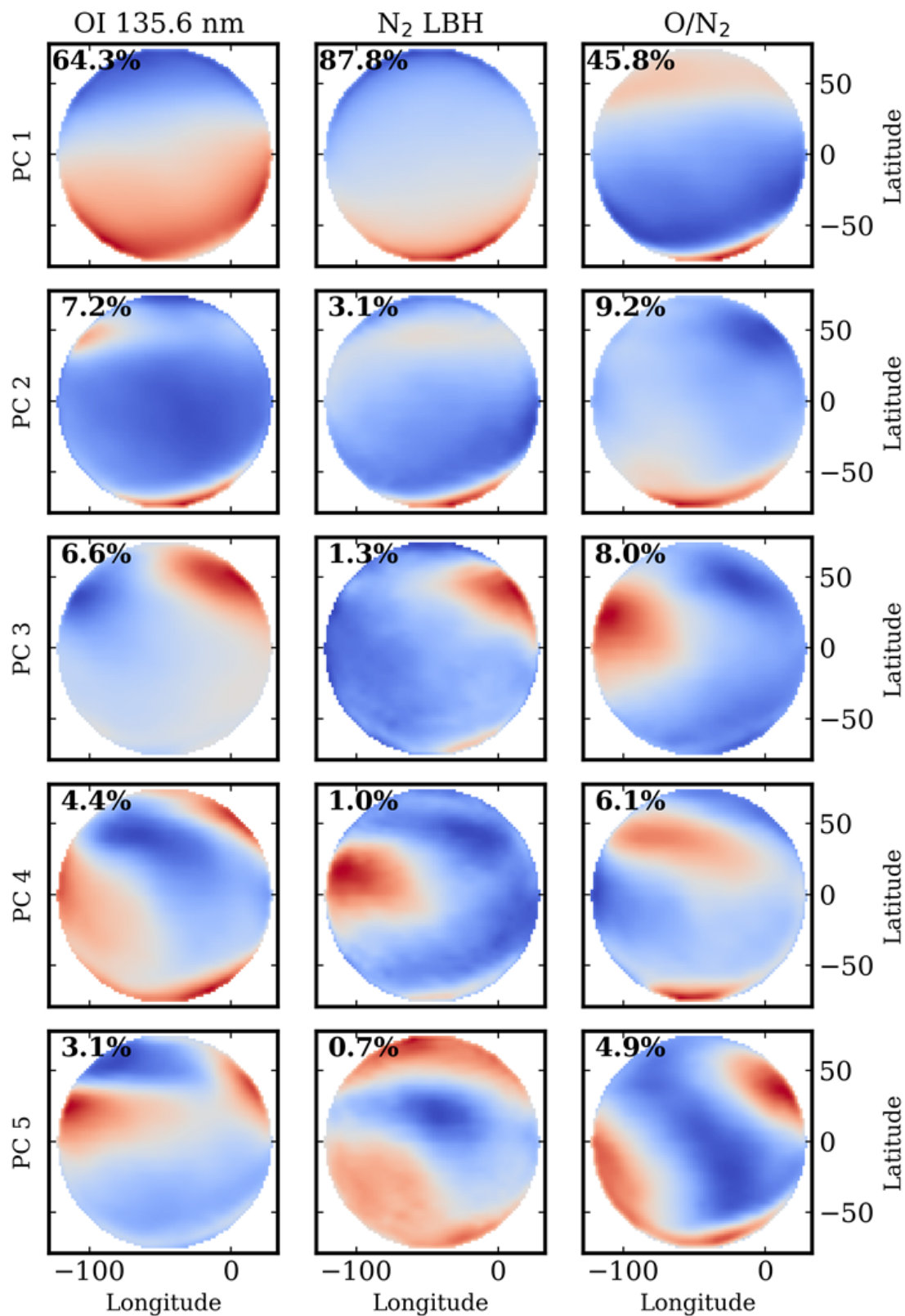
Figure 10: The first five PCs (ranked in order of highest explained variance) for each of the major dayglow observation features as a function of latitude and longitude. The bold value in the top-left corner of each window represents the percent of the total variance explained by that component.

Referring to Figure 10, the five PCs explain 86%, 94%, and 74% of the total variance observed over April for OI 135.6 nm, N_2 LBH, and O/N_2, respectively. PCs 1-2 are most likely driven by geomagnetic conditions. PCs 3-5 may be driven by geomagnetic conditions, lower atmosphere conditions, or a combination of the two.
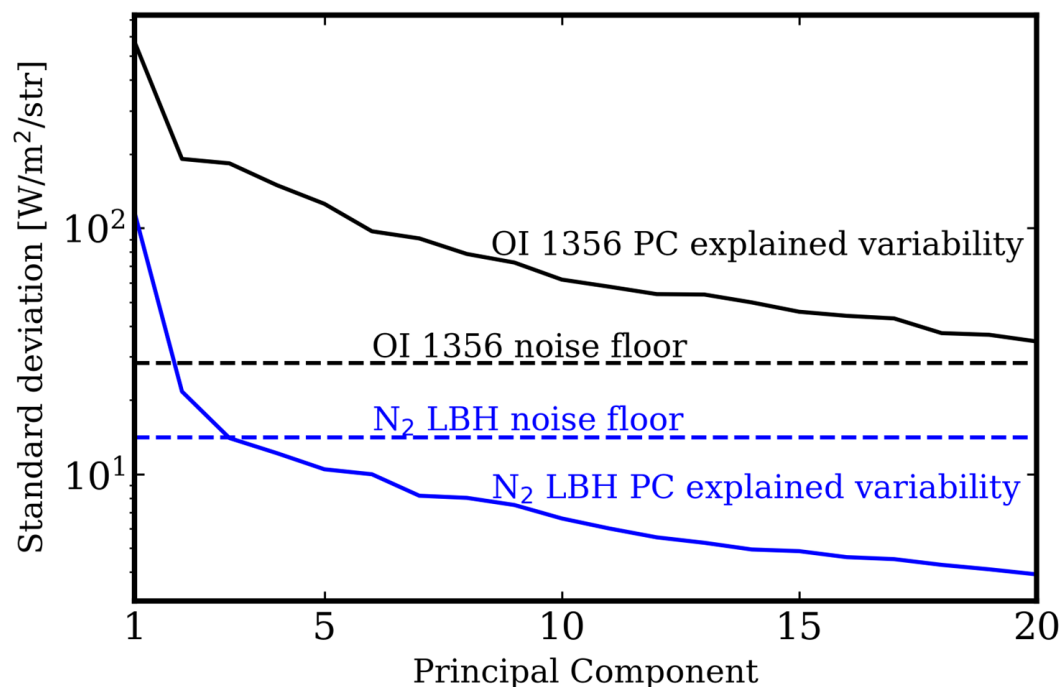

Figure 11: The standard deviation of each of the first 20 principal components for OI 135.6 nm and N_2 LBH emissions. The noise floors that are computed by taking the square root of the mean radiance (Figure 9), assuming Poisson noise, highlight which PCs are theoretically detectable by GOLD.

Figure 11 suggests **GOLD should observe signifcant variability (> 20 PCs are above noise floor) over Earth's disk in OI 135.6 nm due to geomagntic and possbily lower atmosphere forcing, but limited variability (2 PCs above noise floor) only during geomagnetically active periods in N_2 LBH.** These model results are in agreement with recent findings by Immel et al. (2020).

GOLD Observations

PCA is performed on GOLD observations over the same April, 2020 period using observations acquired between 14:30 and 15:30 UT.
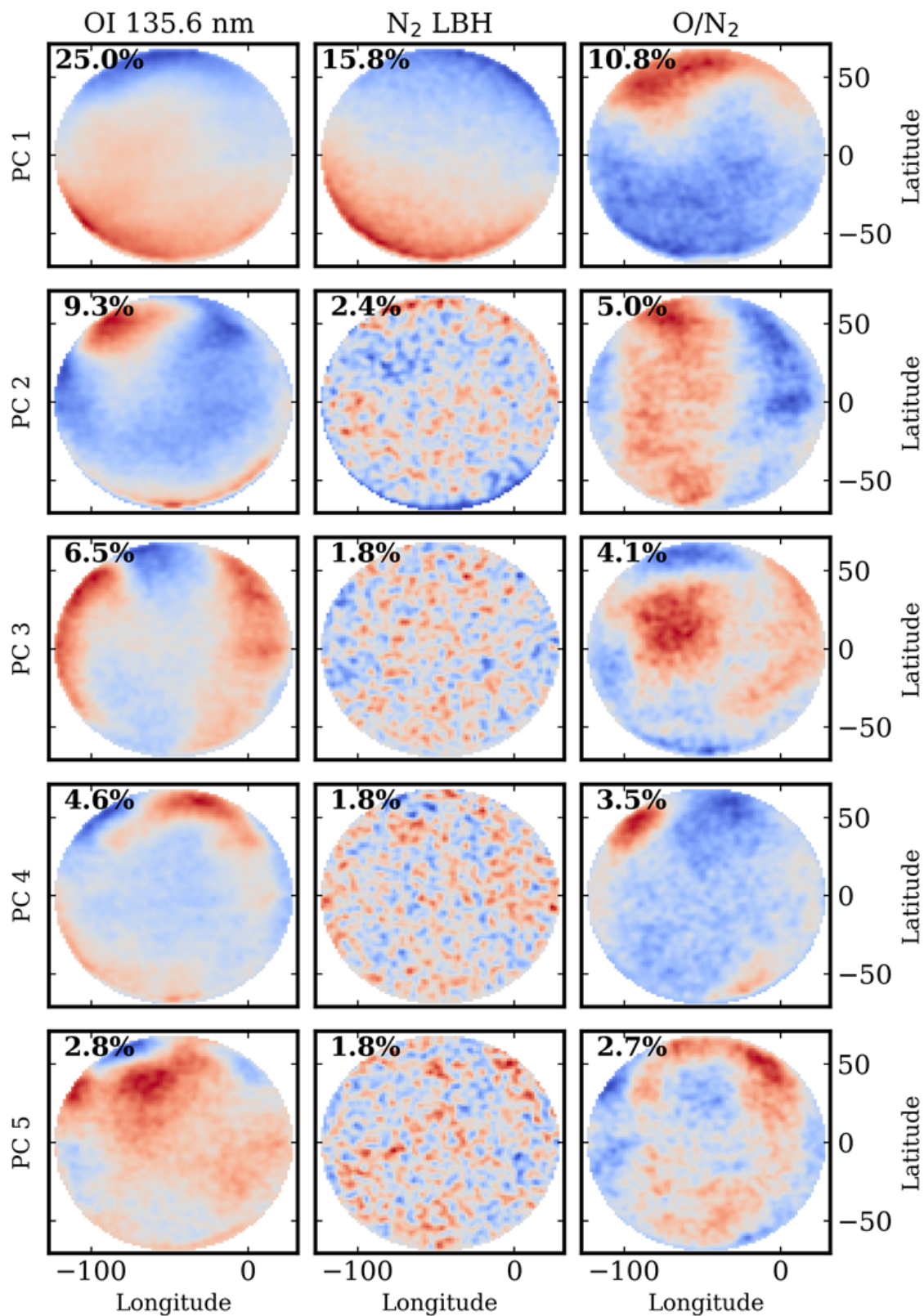
Figure 12: Same structure as Figure 10.

Referring to Figure 12, the first five PCs in the GOLD observations explain 48%, 24%, and 26% of the total variance observed over April for OI 135.6 nm, N_2 LBH, and O/N_2, respectively. This is considerably less than the PCs from the simulated observations (Figure 10) and appears to be primarily attributable to a difference in

percent variance explained of PC 1. **PCs 1-2 show similar morphologies between simulated and GOLD observations for OI 135.6 nm emission. N$_2$ LBH emission only shows one coherent mode of variaiblity, in agreement with comparing model results to the expected noise floor** (Figure 11).

PCA ON FUV AIRGLOW OBSERVATIONS II - SENSITIVITY TO LOWER ATMOSPHERE FORCING VARIABILITY

PCA is performed on simulated observations using all 80 ensemble members from **ENS2** for observations on April 19, 2020 at 15 UT to **determine the major modes of airglow variability due only to lower atmosphere variability.**
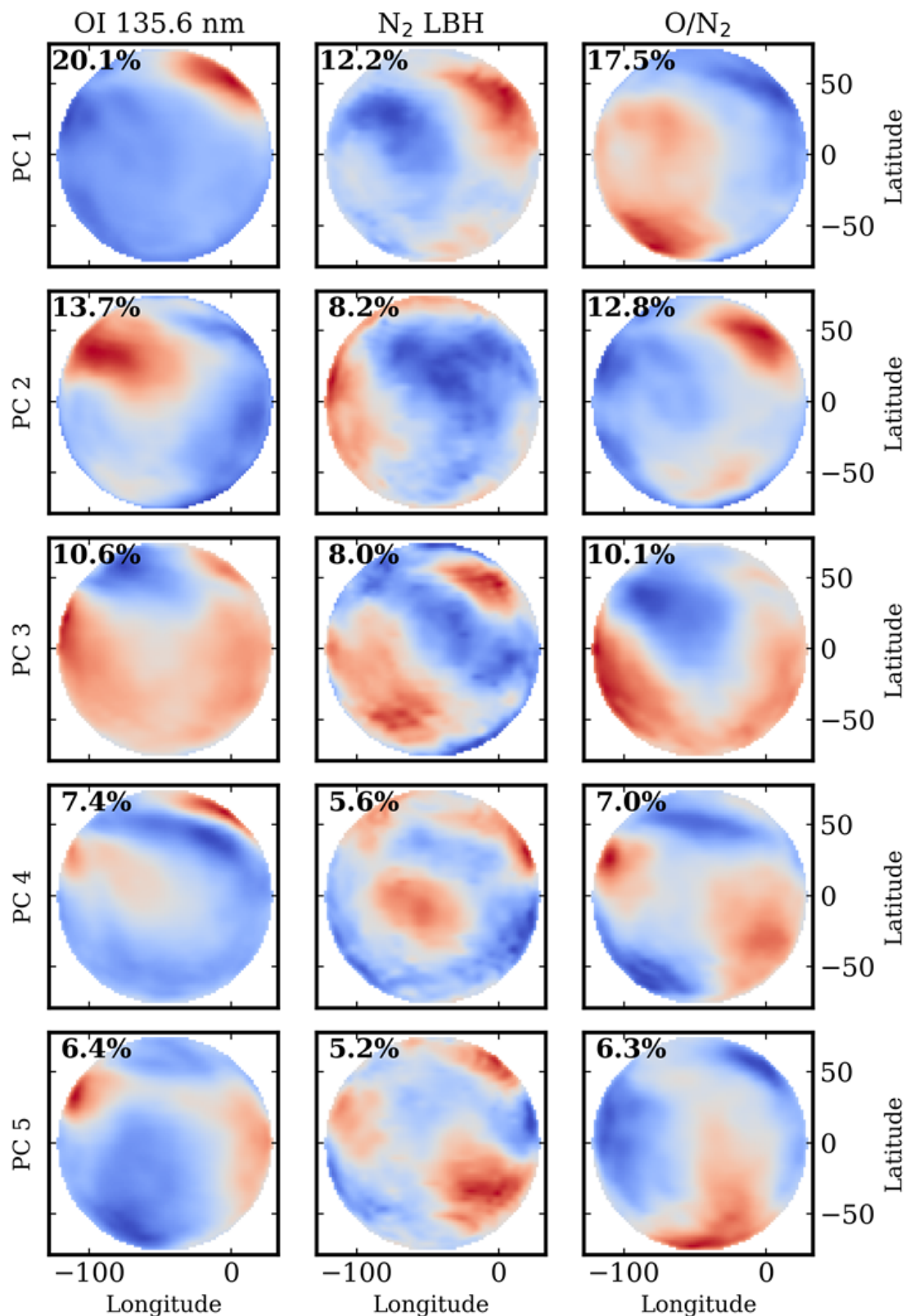
Figure 13: Same structure as Figures 10 and 12.

Referring to Figure 13**, note that the PCs show similar morphologies to PCs 3 and higher in Figure 10 but with noticable differences**. These differences may suggest that PCs 3 and higher in Figure 10 are an combination of lower atmosphere and geomagnetic modes of variability.
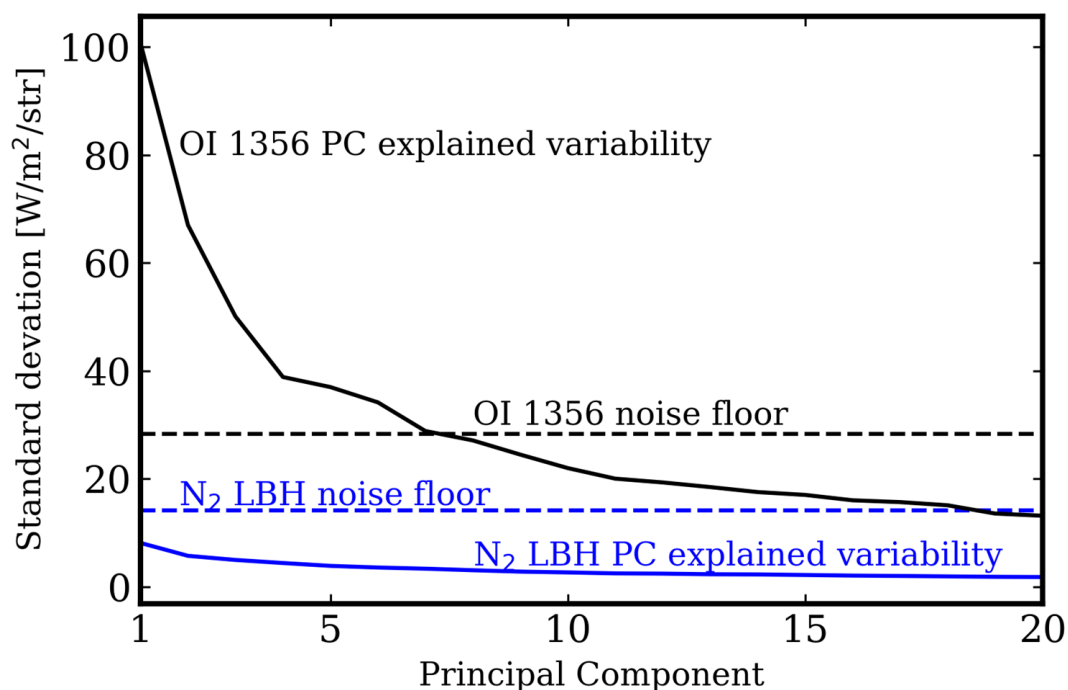

Figure 14: The standard deviation of each of the first 20 principal components for OI 135.6 nm and N_2 LBH emissions.

Figure 14 suggests that 6-7 of the dominant modes of variaiblity in OI 135.6 nm emission due to lower atmopshere forcing should be observable by GOLD. N_2 LBH observations will likely not detect lower atmosphere variations.

SUMMARY

Preliminary Results

1. **Established an ensemble modeling capability with WAM and GLOW**
2. **Performed tidal decomposition on WAM ensemble**
   1. Results to be used in future airglow sensitivity studies
3. **Determined major modes of dayglow (noon LT) variability as a function of latitude and longitude driven by a combination of geomagnetic and lower atmosphere conditions.**
   1. OI 135.6 nm emission shows considerable variability due to both geomagnetic and lower atmosphere forcing
   2. N_2 LBH shows very weak variaiblity with only detectable mode occuring with elevated geomagnetic forcing
   3. Some agreement in both morphology and percent variance explained for major principal components between simulated observations and GOLD observations but also important differences that need further investigation
4. **Detectable modes of OI 135.6 nm variability that are a result of lower atmosphere forcing**

Future Work

This work will be continued with the following pursuits:

1. **PCA as a function of latitude and local time** over expanded universal time rang
2. **Driver-response correlation analysis**
   1. Attribute geomagnetic and lower atmosphere drivers to principal components
3. **Continue airglow-lower atmosphere sensitivty study**
   1. Observability of tidal components
4. **Observing System Simulation Experiment**
   1. Benefits of GOLD constellation

AUTHOR INFORMATION

Clayton Cantrall, Graduate Student, University of Colorado, Boulder (clayton.cantrall@colorado.edu)

Tomoko Matsuo, Assistant Professor, University of Colorado, Boulder (tomoko.matsuo@colorado.edu)

ABSTRACT

Earth's thermosphere is driven by a combination of meteorological, magnetospheric, and solar forcing that exhibits significant variation from day-to-day. The relative importance of these drivers and their combined affects in determining daily thermospheric variability on global and local scales is an important science question particularly under solar minimum conditions. Far-ultraviolet, satellite-based airglow observations are a valuable tool to probe the thermosphere and can provide the spatial coverage and temporal resolution required to improve our understanding of thermospheric day-to-day variability in response to driver variability. This paper presents first results from principal component analysis and ensemble sensitivity analysis to quantify the major modes of dayglow variability in both OI 135.6 nm emissions and N2 Lyman-Birge-Hopfield emissions and the sensitivity of these modes to geomagnetic and lower atmosphere drivers. The ensemble simulations are performed with NOAA's Whole Atmosphere Model that extends from Earth's surface to the exobase and NCAR's Global Airglow Model for a recent period with low-to-moderate levels of geomagnetic activity and low solar activity. The ensemble simulations are compared to thermospheric observations over the same period by the NASA Global-scale Observations of the Limb and Disk (GOLD) mission.

REFERENCES

Akmaev, R. A. (2011), Whole atmosphere modeling: Connecting terrestrial and space weather, Rev. Geophys., 49, RG4004, doi:10.1029/2011RG000364.

Carruthers, G. R., and T. Page (1972), Apollo 16 far-ultraviolet camera/spectrograph: Earth observations, Science, 177, 788–791, doi:10.1126/science.177.4051.788.

Chen, Y.-T., C. H. Lin, C. H. Chen, J. Y. Liu,J. D. Huba, L. C. Chang, H.-L. Liu, J. T. Lin,and P. K. Rajesh (2014), Theoreticalstudy of the ionospheric pla   sma cave inthe equatorial ionization anomalyregion, J. Geophys. Res. Space Physics,119, 10,324?10,335, doi:10.1002/2014JA020235

Chiu Y.T., An Improved Phenomenological Model of Ionospheric Density, J. Atmos. Terr. Phys. 37, 1563, 1975

Eastes, R. W., Solomon, S. C., Daniell, R. E., Anderson, D. N., Burns, A. G., England, S. L., et al. (2019). Global−scale observations of the equatorial ionization anomaly. Geophysical Research Letters, 46, 93189326. doi:10.1029/2019GL084199

Immel, T. J., Sagawa, E., England, S. L., Henderson, S. B., Hagan, M. E., Mende, S. B., Frey, H. U., Swenson, C. M., and Paxton, L. J. (2006), Control of equatorial ionospheric morphology by atmospheric tides, Geophys. Res. Lett., 33, L15108, doi:10.1029/2006GL026161.

Immel, T.J.; Eastes, R.W.; McClintock, W.E.; Mende, S.B.; Frey, H.U.; Triplett, C.; England, S.L. Daily Variability in the Terrestrial UV Airglow. Atmosphere 2020, 11, 1046.

Paxton, L. J., Schaefer, R. K., Zhang, Y., and Kil, H. (2017), Far ultraviolet instrument technology, J. Geophys. Res. Space Physics, 122, 2706– 2733, doi:10.1002/2016JA023578.

Solomon, S. C. (2017), Global modeling of thermospheric airglow in the far ultraviolet, J. Geophys. Res. Space Physics, 122, 7834– 7848, doi:10.1002/2017JA024314.